4th URSI AT-RASC, Gran Canaria, 19-24 May 2024

Non-metallic object detection by 3D MIMO radar for security inspections

Naruto Yonemoto, Akiko Kohmura, Shunichi Futatsumori, Kazuyuki Morioka, Masahiko Sato, and Norihiko Miyazaki
Electronic Navigation Research Institute, National Institute of Maritime, Port and Aviation Technology, Tokyo, Japan

Abstract

A new security inspection system under development transmits the radio wave from plural transmitters equipped in a box. To detect non-metallic objects imitating the explosives, the reflection characteristics can be measured. The probability of the reflected power is lower than the reference target for the health check of the conventional inspection systems. The prototype of the 3D MIMO radar detects the objects and creates a clear radar image for the objects..

1. Introduction

The demand for security inspection is highly increasing to protect people from terror attacks. Within the restricted area in the airport, the duty on the inspection is issued by the international treaty. Under these conditions, many trials have been conducted [1-4], and some advanced inspection systems have been provided the service to detect concealed objects in the airport [5, 6]. To evaluate the ability of the detection of suspicious items, the airport operator sometimes runs blind tests to check the detection performance of the objects which imitate the explosives. However, even a large portion of the imitations results in quite low detectability using various types of conventional systems. To overcome these situations, a new MIMO radar is under development [7].
This paper introduces the structures of the MIMO radar with the plural transmitter emitting the signal simultaneously and the fundamental performance of the imaging for the metallic object is introduced. The RCS measurement for the various samples is discussed. Finally, the imaging results of the radar are also provided.

2. Prototype of MIMO imaging radar for security inspections

The prototype of the MIMO imaging radar is shown in Figure 1. The system has a vertical array for the transmitters and a horizontal array for the receivers. The control board generates the FMCW signal and distribute the signal to the transmitting and receiving arrays. In the transmitter array, the FMCW signal is upconverted to a pulse with the linear sweep in the dual-band operations. Each pulse is transmitted in-phase or reversed phase by the bit of the ID code for each transmitter. The reflected signal is captured by the receiver as the mixture of the reflected signals from all transmitters. Using the series of the pulse, the signal processing produced the transformation from pulse number to the response to the transmitters.

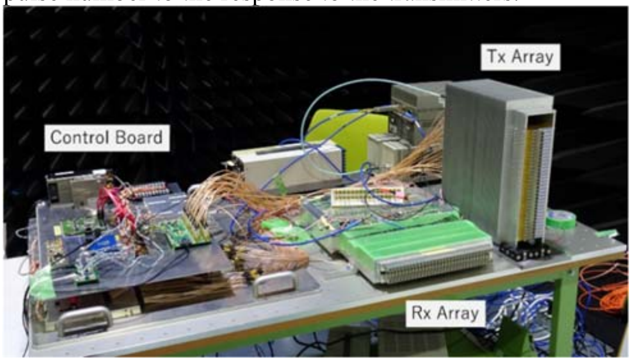

Figure 1. Overview of the prototype of 3D MIMO radar.

The image reconstruction method is illustrated in Figure 2. Using the combination of 32 transmitters and 32 receivers, 1024 range responses are generated. After obtaining the responses, three-dimensional scattering images are calculated using the following formula:

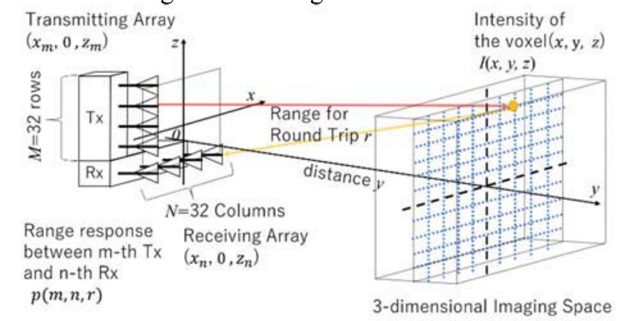

Figure 2. Calculation schemes of 3D radar imaging

$$I(x, y, z) = \sum_{m=1}^{M} \sum_{n=1}^{N} p(m, n, r) * e^{j\theta} \quad (1).$$

The voxel's intensity in the 3D imaging space is calculated by summating the extracted range response according to the actual propagation length with the compensation of the phase rotations. The calculation results are 3D coordination of the scattered signals. A perspective view of the 3D data is shown in Figure 3. A concealed gun under the jacket is detected in this case. Detailed structure and the measurement method are described in [7].

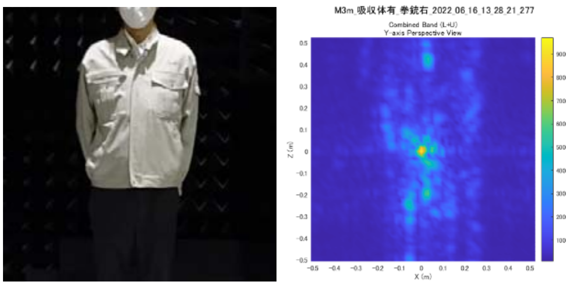

Figure 3. Typical detection results for concealed metallic gun under the jacket(the left figure is the photograph of the inspected person, right figure is the perspective view of the 3D radar image calculated by Equation (1).

3. Reflection analysis of the non-metallic objects in the RCS measurements

In the operation of the aircraft, the total damage to the airframe is the worst scenario of the attack. A large portion of the explosives may cause the rupture of the pressured cabin space. To detect such suspicious items, several samples are prepared. The tested samples are shown in Figure 4. Four imitations for the explosives are made of sugar which has a similar dielectric constant to the major explosive materials [8]. The reference objects used for the daily check of the system in the airport are also measured. In the first phase of the analysis, the intensity of the reflection from the objects is measured using the vector network analyzer (VNA). The operating frequency of the system A [5] is 75GHz and that of the system B [6] is 24 GHz. The test setup for each frequency band is shown in Figure 5. The antenna for transmission is connected to port 1 and the reception antenna is connected to port 2 of the VNA. The appropriate accessories are used for each frequency band.

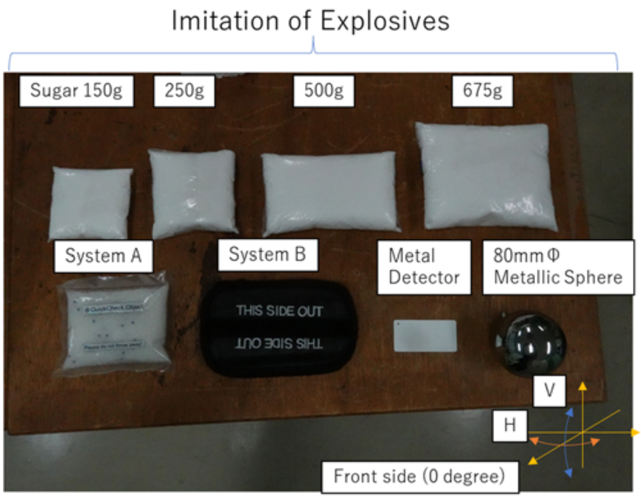

Figure 4. Tested samples (4 imitations of explosives with different portions of sugar, 3 reference objects for the daily checks in the airport, and a metallic sphere with 80 mm of diameter for the calibration of the reflection).

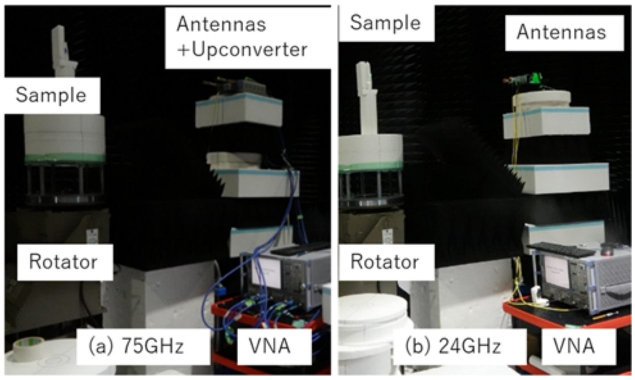

Figure 5. RCS test setup using the VNA.

All tested samples are placed on the rotator and the front side faces the antenna side. Changing the incident angle, the frequency characteristics are measured. The RCS of the all-tested samples are measured in both frequency ranges. The VNA measured the frequency response by changing the incident angle of the object. The time domain responses are calculated by the inverse FFT from the frequency responses. A typical measured result in the front side direction is shown in Figure 6. Two peaks are observed within the 10ns of the time scales. The first peak corresponds to the antenna coupling and the second peak is the reflection from the tested objects. The strength of the peak is normalized by the strength of the reference metallic sphere with -22 dBsm of the RCS. The calibrated RCS characteristics for the samples for the daily check are shown in Figures 7 and 8. Assuming the daily check in the airport, the metallic plate for the test ofthe conventional metal detector is also measured and shown in Figure 9. The reference objects for the daily checks have wider angular characteristics in both directions of the incident angles. It means that they are quite easy to detect without any consideration of the placement of the object. In the case of metallic plates, the narrow and strong peaks are observed in the front side direction. The broadside reflection was observed by the rounded edges of the plates. A large portion of the imitation is also shown in Figure 10. Some null angles are observed but a significant difference is not recognized in the graph.

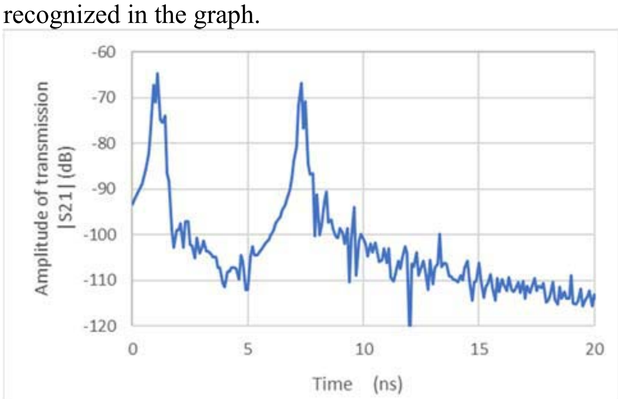

Figure 6. Time domain response for the small portion of the imitation in the front side.

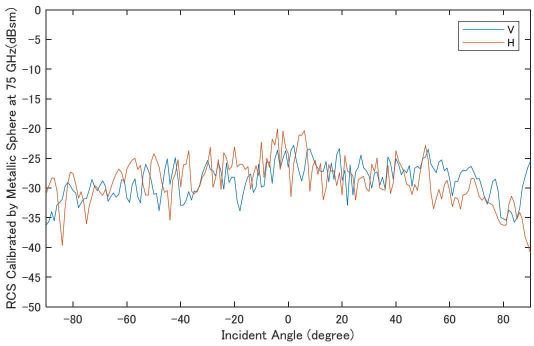

Figure 7. Angular characteristics of the reference target for system A in its operating frequency.

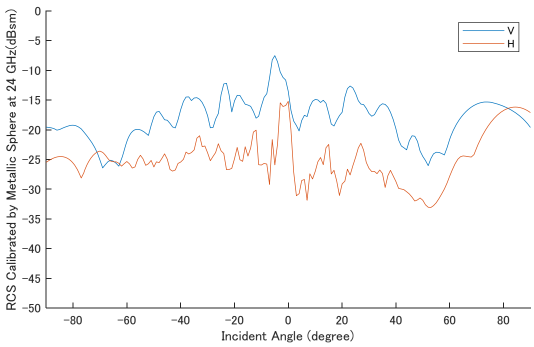

Figure 8. Angular characteristics of the reference target for system B in its operating frequency.

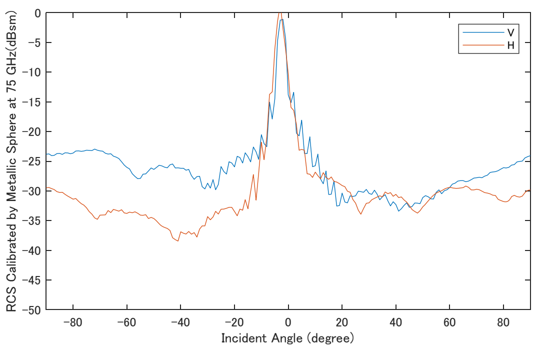

Figure 9. Angular characteristics at 75 GHz of the metallic plate for the conventional metal detector operating in the airport.

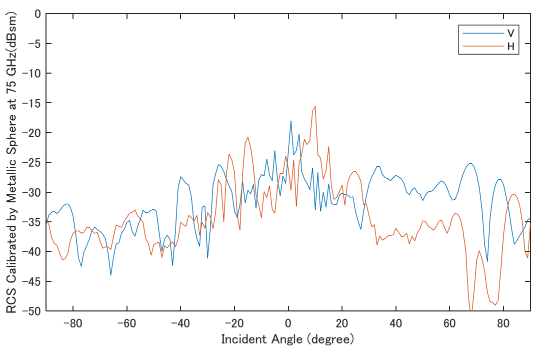

Figure 10. Angular characteristics of RCS for the large portion of the imitations with the 180-degree variations of incident angle (observing point).

4. Statistical features of RCS

To find the difference between the tested samples, the probability of the RCS of each sample is calculated. Figure 11 shows the cumulative distribution functions of the measured RCS for each sample in the 75 GHz band. The CDF of the imitations is placed on the left side of the figure. It means the RCS of the imitation might have a lower reflection in comparison to the reference target. For example, the detection threshold values are set to -35 dBsm for system A, the detection probability of the reference target is around 95 % (misdetection rate 5%) and that of smallest imitation is around 10% (misdetection rate 90%). That is the reason why the system couldn't detect the imitations.

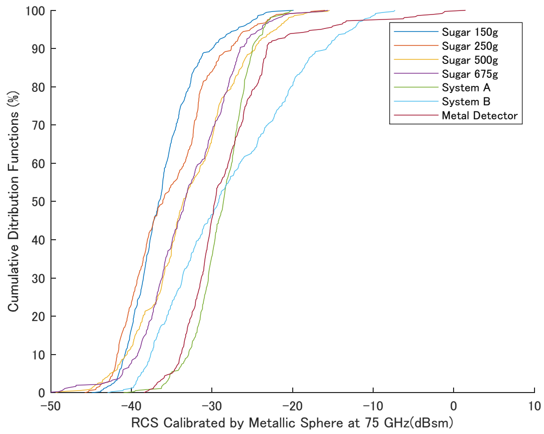

Figure 11. Cumulative distribution functions of the RCS of tested samples at 75GHz (operating frequency of the system A)

In comparison to system B, the cumulative distributions of all tested samples at 24 GHz are shown in Figure 12. The CDF of the reference target for system B records quite a high RCS value in the operating frequency. As a result, the low detection probability for the imitations is analyzed.

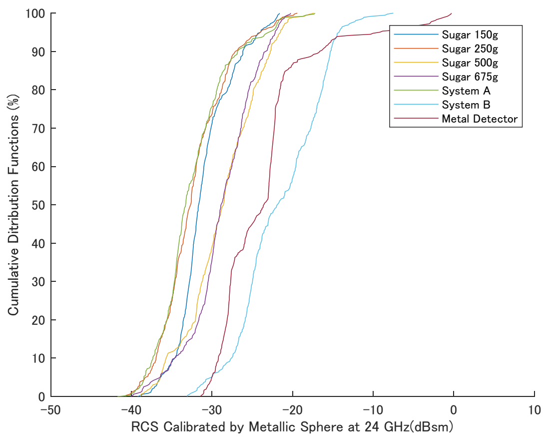

Figure 12. Cumulative distribution function of the RCS of tested samples at 24 GHz (operating frequency of the system B)

5. 3D radar imaging for detection

In order to increase the detection probabilities, the inspection methods should be changed. At least, several screenshots with changing the incident angles are needed to be obtained to identify the concealed object. The preliminary results of 3D radar imaging for the front side of the tested samples located at the 1m distance are shown in Figure 13.

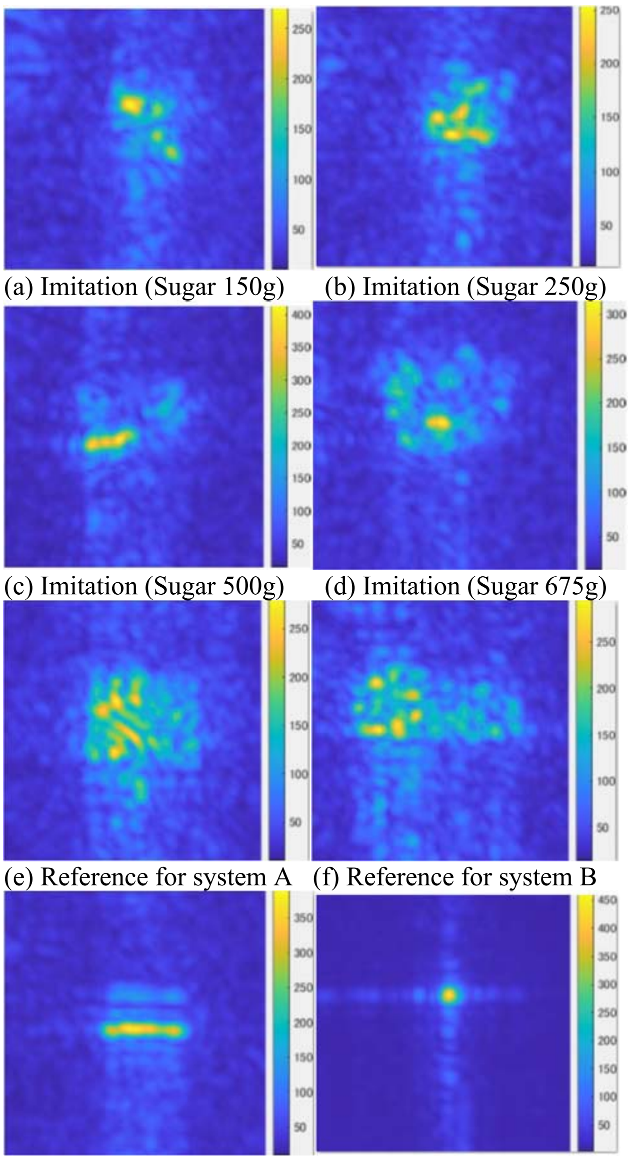

(a) Imitation (Sugar 150g) (b) Imitation (Sugar 250g)
(c) Imitation (Sugar 500g) (d) Imitation (Sugar 675g)
(e) Reference for system A (f) Reference for system B
(g) Metallic plate (h) 80mm sphere

Figure 13. Perspective views of 3D radar image for the test samples.

The vertical and horizontal size of the image is 300 mm Using the prototype system, the front side image is completely reconstructed. For the referenced target, the shape and size of the objects are equally reconstructed. However, the outline of the shape is not clear for all imitation measurements. The image is greatly changed with the rotation of the object. It means that the change of the measurement angle is required for the precise detection.

6. Conclusion

This paper shows the theoretical analysis of the various test samples for the security inspection systems. The test results show that the intensity of RCS greatly differs between the samples for the daily check and non-metallic objects.

7. Acknowledgements

This work is supported by the Ministry of Land, Infrastructure, Transportation, and Tourism.

References

[1] Z. Wang, et al., “Review of Active Millimeter Wave Imaging Techniques for Personnel Security Screening,” IEEE Access, Vol. 7, pp. 148336-148350, 11 October, 2019

[2]S. S. Ahmed, et al. , “Advanced Microwave Imaging,” IEEE Microwave Magazine, Volume: 13, Issue: 6, Sept.-Oct. 2012

[3] K. Mizuno , et al., “Millimeter-Wave Imaging Technologies and Their Applications,” 2007 IEEE International Vacuum Electronics Conference, 15-17 May 2007

[4] E. Kpre, et al., “A Compressive Millimeter-Wave Interferometric Imager for Security Applications,” 2018 IEEE International Symposium on Antennas and Propagation & USNC/URSI National Radio Science Meeting, 8-13- July, 2018

[5] Rohde & Schwarz, “R&S®QPS quick personnel security scanner,” https://www.rohde-schwarz.com/products/aerospace-defense-security/security-scanner/rs-qps-quick-personnel-security-scanner_63493-332676.html?change_c=true

[6] Leidos, “People Scanning -Provision 2-,” https://www.leidos.com/markets/aviation/security-detection/aviation-checkpoint/people-screening

[7] N. Yonemoto, et al., “Improvement of Depth Resolution by Dual-Band Integration for 3D MIMO Radar for Security Inspections,” Proc. of Conference on Antenna Measurement and Applications (CAMA 2023), 15-17 November, 2023

[8] L P. O. Robitaille, et al. , “Dielectric constant predictions for energetic materials using quantum calculations,” Defense Technologies, vol. 17 issue 6, pp.1988-1994, December 2021